# Investigation of the electrical properties of $SnO_2$ varistor system using impedance spectroscopy

P. R. Bueno
*Departamento de Química, UFSCar, C.P. 676, 13565-905 São Carlos, SP, Brazil*

S. A. Pianaro
*Departamento de Engenharia de Materials, UEPG, 84031-510 Ponta Grossa, PR, Brazil*

E. C. Pereira,[a] L. O. S. Bulhões, and E. Longo
*Departamento de Química, UFSCar, C.P. 676, 13565-905, São Carlos, SP, Brazil*

J. A. Varela
*Instituto de Química, UNESP, C.P. 355, 14800-900 Araraquara, SP, Brazil*

(Received 6 December 1996; accepted for publication 1 July 1998)

The electrical properties of tin oxide varistors doped with CoO, $Nb_2O_5$, and $Cr_2O_3$, were investigated using the impedance spectroscopy technique with the temperature ranging from 25 to 400 °C. The impedance data, represented by means of Nyquist diagrams, show two time constants with different activation energies, one at low frequencies and the other at high frequencies. These activation energies were associated with the adsorption and reaction of $O_2$ species at the grain boundary interface. The Arrhenius plots show two slopes with a turnover at 200 °C for both the higher and lower frequency time constants. This behavior can be related with the decrease of minor charge carrier density. The barrier formation mechanism was associated with the presence of $Cr_{Sn}^{\cdot}$ at the surface, which promotes the adsorption of the $O'$ and $O''$ species which are in turn proposed as being responsible for the barrier formation. © *1998 American Institute of Physics.* [S0021-8979(98)04719-7]

## INTRODUCTION

$SnO_2$ has a tetragonal structure, similar to the rutile structure, and behaves as an *n* type semiconductor.[1] This oxide has been extensively described in the literature because of its importance as a gas and humidity sensor.[2–4] These properties, along with electrical ones, are dependent on the surface nonstoichiometry produced by the powder preparation, by the thermal treatment and by the atmosphere present in the oven during the preparation of the material.[2–4] The double Schottky barrier is known to form at the grain boundary region by oxygen or hydroxyl adsorption during the sintering process.[5] The problems related to the preparation of dense $SnO_2$ restrict the investigation to the sensor properties. Recently, CoO addition to the $SnO_2$ was observed to lead to 98.5% of theoretical density and made possible the application of these systems in the preparation of varistors.[6]

The electrical behavior of a varistor is represented by the nonohmic relation:

$$J = KE^{\alpha}, \tag{1}$$

where $J$ is the current density, $E$ the electrical field, $K$ a constant related to the material resistance, and $\alpha$ is the nonlinear coefficient ($\alpha > 1$). Varistors are used as surge arrestors and voltage transient protecting devices for electronic and industrial equipment.

The objective of this article is to investigate the electrical properties and barrier formation mechanism of the varistor systems $SnO_2.CoO.Nb_2O_5$ (SCN) and $SnO_2.CoO.Nb_2O_5.Cr_2O_3$ (SCNCr) using the impedance technique.

## EXPERIMENTAL PROCEDURE

The powder mixture was ball milled in alcohol. The following oxides were used: $SnO_2$ (Merck), CoO (Riedel), $Nb_2O_5$ (Aldrich), and $Cr_2O_3$ (Vetec).

The molar compositions investigated were: 98.95% $SnO_2$+1.0% CoO+0.05% $Nb_2O_5$ (SCN) and (98.95%–*X*%) $SnO_2$+1.0% CoO+0.05% $Nb_2O_5$+*X*% $Cr_2O_3$ (SCNCr), with *X* equal to 0.05%, 0.1%, 0.3%, and 0.5%.

The powder was pressed to obtain pellets (10.5 mm ×1.0 mm) by uniaxial pressing (20 MPa) followed by isostatic pressing at 210 MPa. The pellets were sintered at 1300 °C for 1 h followed by cooling at 3 °C/min. Grain sizes were determined by analyzing scanning electron microscopy (SEM) micrographies using the intercept method.

In order to make the electrical measurements, silver contacts were deposited on sample surfaces, and then the pellets were heated at 500 °C during 1 h.

The impedance measurements were made with a frequency response analyzer (Solartron model 1260) using frequencies ranging from 100 Hz up to 4 MHz, with an amplitude voltage of 1 V. The pellets were put in a sample holder[7] attached to a furnace (EDG model EDGCON 3P). Measure ments were made at temperatures ranging from 25 to 400 °C.

[a]Author to whom correspondence should be addressed. Electronic mail: decp@power.ufscar.br

 

TABLE I. Grain size of systems SCN and SCNCr sintered at 1300 °C for 1 h.

| Molar system composition (%) | Nonlinear coefficient | Grain size ($\mu$m) |
|---|---|---|
| 0.00 | 8 | 7.50 |
| 0.05 | 41 | 5.40 |
| 0.10 | ··· | 4.50 |
| 0.30 | ··· | 3.10 |
| 0.50 | ··· | 2.40 |

The impedance data were analyzed with the EQUIVCRT program.[8]

## RESULTS

A recent article[6] has described the dc electrical behavior of the SCN and SCNCr systems as a function of different $Cr_2O_3$ molar concentrations. SCN presents a varistor behavior with $\alpha=8$ and a breakdown electric field ($E_B$) of 1870 V cm$^{-1}$. When 0.05% $Cr_2O_3$ was added to the system, the $\alpha$ value increased to 41 and the breakdown field to 3990 V cm$^{-1}$. Furthermore, higher levels of $Cr_2O_3$ led to a deleterious effect on the varistor behavior, since the $E_B$ could not be detected in these ceramic compositions. Table I shows the decrease of the grain size when $Cr_2O_3$ at different concentrations was added.

Figure 1 shows the Nyquist diagrams of SCNCr with 0.05% $Cr_2O_3$ at three different temperatures. In Fig. 1 two semicircles partially convoluted are observed which indicate the presence of two time constants in the system. The electrical response can be fitted by an equivalent electrical circuit composed by two series circuits of a resistance and capacitor in parallel, as shown in Fig. 2(b). At this point it is important to discuss the model used for the fitting procedure. The results shown in Fig. 1 do not always suggest the existence of two time constants. For such results, the best criterion to verify the validity of the proposed model is the use of the chi squared parameter of the nonlinear least square procedure.[8] Figure 3 shows the data for SCNCr with 0.05% of $Cr_2O_3$ together with the calculated simulated parameters, using one time constant [Fig. 2(a)] and two time constants [Fig. 2(b)]. Clearly the two time constant model fits the results better than the one time constant model. As it is shown in Table II, the chi squared data calculated from the results presented in Fig. 3 are one order of magnitude lower when the two time constant model is used. Two semicircles in the Nyquist diagram for varistor systems were presented in the literature,[9] however, no discussion was developed concerning the nature of this response.

Figure 4 presents the Bode diagrams for the SCN and SCNCr systems with different $Cr_2O_3$ concentrations at 250 °C. When 0.05% $Cr_2O_3$ is added to SCN an increase on the system resistivity is observed by at least two orders of magnitude at ambient temperature, both for the high and low frequency time constants. These resistivity differences decrease as the temperature is increased, thus indicating higher activation energy for the SCNCr 0.05% when compared to

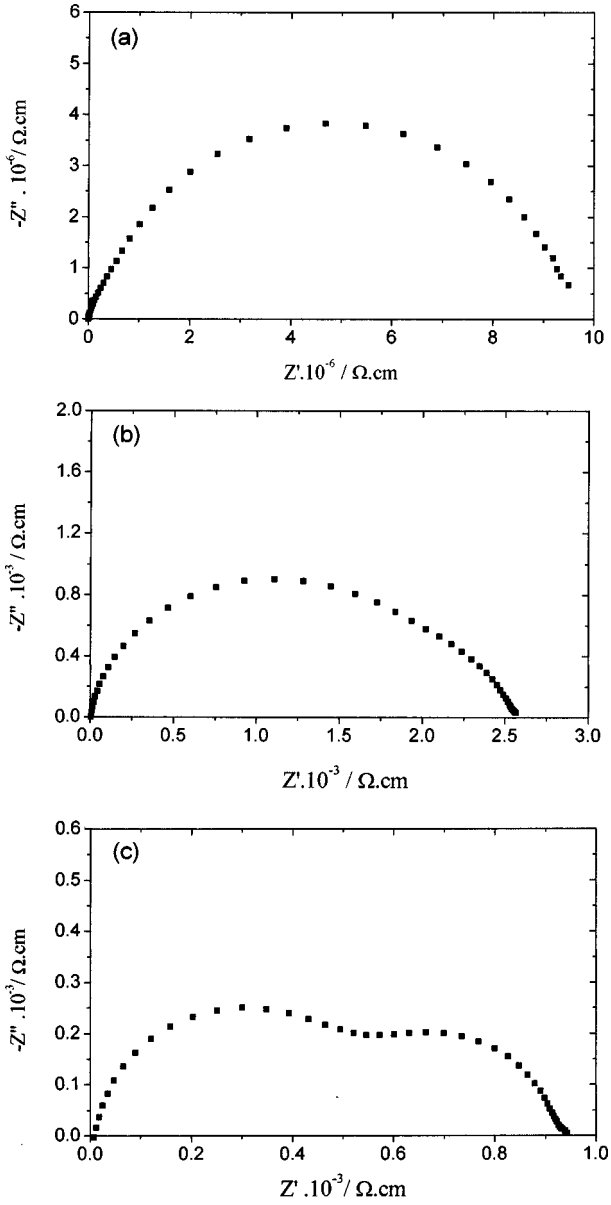


FIG. 1. Nyquist diagrams for SCNCr with 0.05% of $Cr_2O_3$ at different temperatures. (a) 150, (b) 350, (c) 400 °C.

SCN. For $Cr_2O_3$ concentrations higher than 0.05% (such as 0.1%, 0.3%, and 0.5%) an increase in the system resistivity is observed, although no substantial difference in resistivity was detected at room temperature. Figure 5 presents the high and low frequency region capacitances as a function of the temperature for all of the investigated samples. In Fig. 5, the capacitances for $Cr_2O_3$ concentrations higher than 0.05% are two orders of magnitude lower than for SCN and SCNCr 0.05%, which is probably associated with the increase in the grain boundary barrier width. The accumulation of defects in the grain boundary barrier region can lead to this widening, thus decreasing the grain boundary capacitance.

Figures 6 and 7 present the Arrhenius plots for high and low frequencies, respectively. These figures show the presence of two linear regions with different slopes. The slope

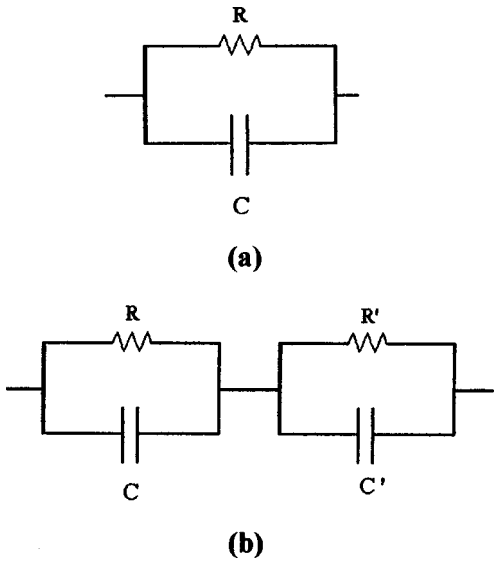


FIG. 2. Equivalent circuit used to fit the impedance data. (a) one time constant; (b) two time constant.

change, in the two cases, occurs at 200 °C. Tables III and IV present the activation energies for the two processes as a function of $Cr_2O_3$ composition calculated from the data presented in Figs. 6 and 7.

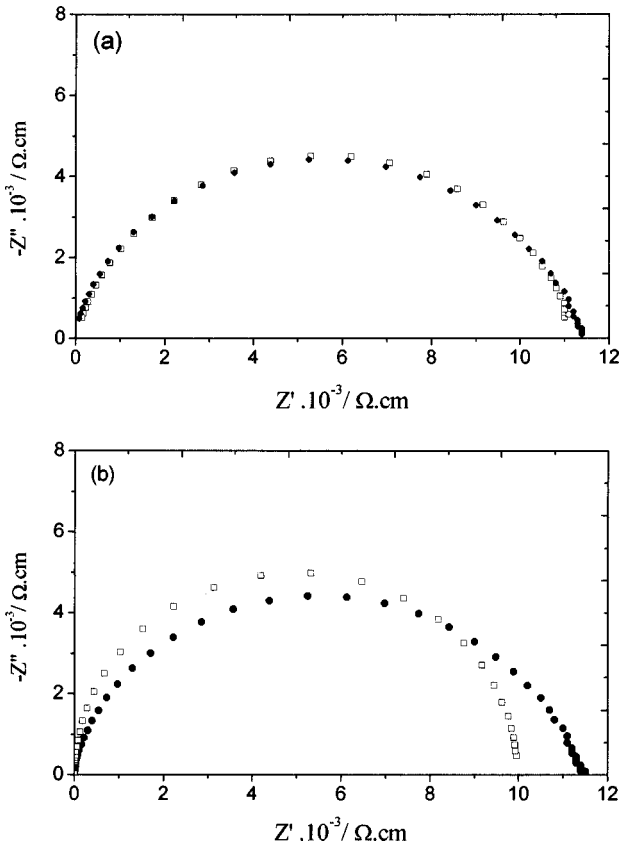


FIG. 3. The Nyquist diagrams for SCNCr with 0.05% of $Cr_2O_3$. (○) Data fitting using the two time constant model; (□) Data fitting using one time constant model; (▲) experimental data.

TABLE II. Parameters calculated of SCNCr with 0.05% of $Cr_2O_3$ at 300 °C by the one time constant model and the two time constants model.

| Two time constants model | | One time constant model | |
|---|---|---|---|
| chi squared $=1.3\times10^{-4}$ | | chi squared $=1.7\times10^{-3}$ | |
| Parameters | Value | Parameters | Value |
| $R$ | $7.9\times\ 10^{3}$ | $R$ | $1.1\times\ 10^{4}$ |
| $C$ | $3.7\times10^{-9}$ | $C$ | $2.6\times10^{-9}$ |
| $R'$ | $3.3\times10^{-3}$ | ⋯ | ⋯ |
| $C'$ | $1.8\times10^{-9}$ | ⋯ | ⋯ |

## DISCUSSION

Two hypotheses may be considered to explain these two time constants:

(a) One time constant is related to the grain boundary barrier and the second is associated with the grain barrier. The weakness of this model is that the grain resistivity thus calculated is at least four orders of magnitude higher than the literature values for grain resistivity of $SnO_2$.[10]

(b) The second hypothesis supposes the existence of different defects and/or adsorbed species at the grain boundary region, not necessarily at the same grain boundary. The two time constants are due to these kinds of defects. The second hypothesis is more probable, since the possibility of existence of different adsorbed species and defects on $SnO_2$ was described in the literature.[11–14]

The presence of dopants leads to the formation of the following defects in the $SnO_2$ structure:

$$CoO \xrightarrow{SnO_2} Co''_{Sn} + V_O^{\cdot\cdot} + O_O^x, \tag{2}$$

$$Co_2O_3 \xrightarrow{SnO_2} 2Co'_{Sn} + V_O^{\cdot\cdot} + 3O_O^x, \tag{3}$$

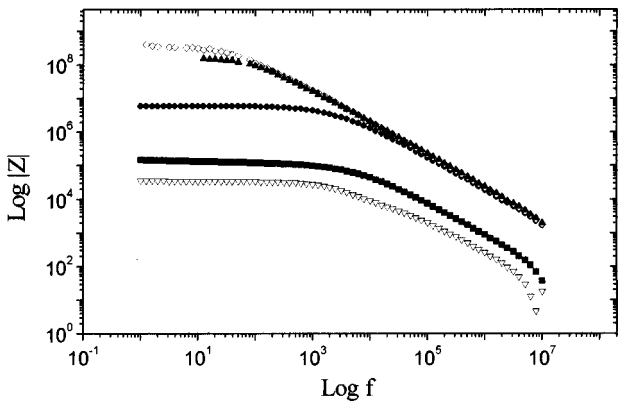


FIG. 4. Impedance as function of frequency logarithm diagrams for SCN and SCNCr systems with different concentration of $Cr_2O_3$ sintered at 1300 °C for 1 h. The impedance measurements were made at temperature of 250 °C. (▽) 0.00% $Cr_2O_3$; (■) 0.05% $Cr_2O_3$; (●) 0.1% $Cr_2O_3$; (◇) 0.3% $Cr_2O_3$; (▲) 0.5% $Cr_2O_3$.

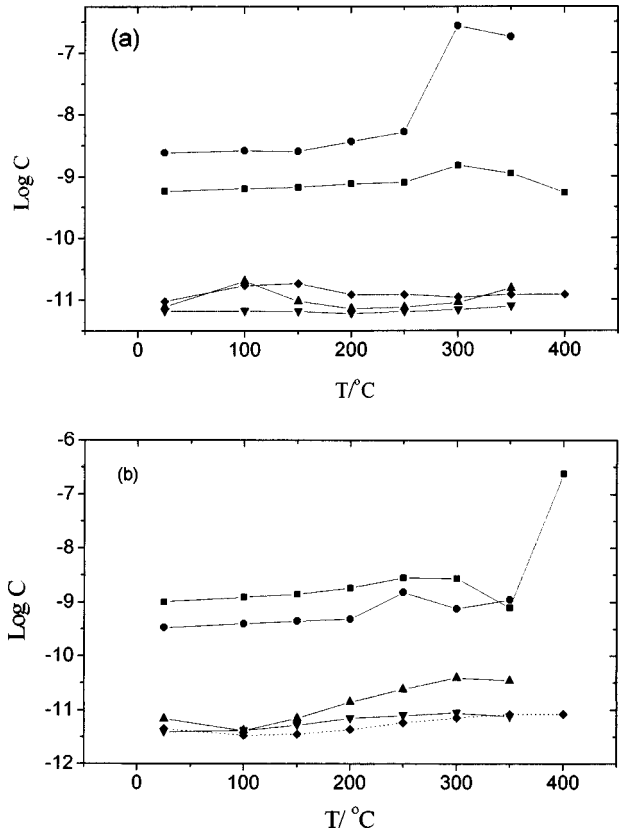


FIG. 5. Capacitance as a temperature function for both (a) high and (b) low frequency regions for the SCNCr systems with the following $Cr_2O_3$ %: (■) 0.00%; (●) 0.05%; (▲) 0.10%; (▼) 0.30%; (◆) 0.50%.

$$2Nb_2O_5 \xrightarrow{SnO_2} 4Nb_{Sn}^{\cdot} + V_{Sn}'''' + 10O_O^x, \tag{4}$$

$$Cr_2O_3 \xrightarrow{SnO_2} 2\ Cr_{Sn}' + V_O^{\cdot\cdot} + 3O_O^x. \tag{5}$$

The defects generated by the presence of $Nb_2O_5$ form a solid solution with $SnO_2$ and lead to an improvement in the grain conductivity. The importance of CoO defects is the creation of $V_O^{\cdot\cdot}$ in the grain boundary region, which is fundamental for the sintering process.[15] On the other hand, the presence of $Co_{Sn}'$ and $Co_{Sn}''$ leads to barrier formation in the grain boundary region, since in the SCN system $\alpha = 8$. The

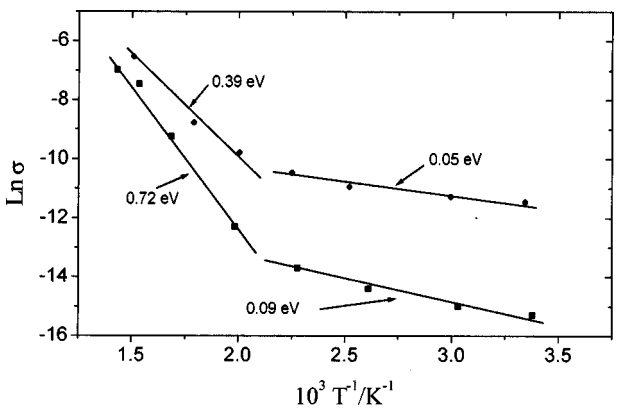


FIG. 6. Arrhenius plots for the high frequency region. (●) 0.00% $Cr_2O_3$; (■) 0.05% $Cr_2O_3$.

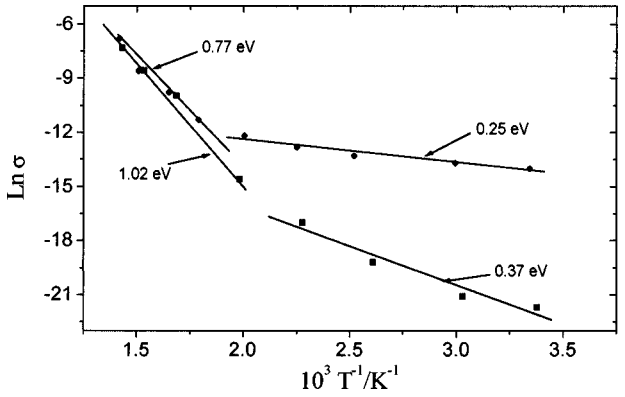


FIG. 7. Arrhenius plots for the low frequency region. (●) 0.00% $Cr_2O_3$; (■) 0.05% $Cr_2O_3$.

defects generated by these two dopants are necessary for a varistor system. However, building up a high and narrow potential barrier at the grain boundary is the last condition required for obtaining a varistor with a high nonlinear $\alpha$ coefficient. The data obtained show that doping the SCN system with $Cr_2O_3$ at a level of 0.05% builds up an optimized barrier at the grain boundary. For $Cr_2O_3$ concentrations higher than 0.05%, the system loses its nonlinearity. This effect is possibly related to a reaction between $Cr_2O_3$ and CoO forming $CoCr_2O_4$, which inhibits the $SnO_2$ grain growth and annihilates the voltage barrier. However, the $Cr_{sn}'$ is not enough to justify the two time constants observed in the impedance data. These results indicate that there are at least two kinds of defects or adsorbed species at the grain boundary region with different activation energies.

Kim *et al.*[16] observed that the activation energies for the O′ and O″ species on the $SnO_2$ surface are 0.6 and 1.0 eV, respectively. These energies are almost equal to those observed in the present article (0.7 and 1.0 eV) for the SCNCr compounds at temperatures higher than 200 °C, as can be seen in Tables III and IV. Then, it is possible that these species predominate at the grain boundary structure and its formation can be represented by the following reactions:

$$Cr_{Sn}' + O_2 \xrightarrow{SnO_2} Cr_{Sn}'.O_{2(ads)}, \tag{6}$$

$$Cr_{Sn}'.O_{2(ads)} \xrightarrow{SnO_2} Cr_{Sn}^{x}.O_{2(ads)}', \tag{7}$$

$$Cr_{Sn}^{x}.O_{2(ads)}' + Cr_{Sn}' \xrightarrow{SnO_2} (Cr_{Sn}^{x})_2.O_{2(ads)}'', \tag{8}$$

TABLE III. Activation energies calculated from the Arrhenius plot at low and high frequency region for the temperature range lower than 200 °C.

| Molar system composition (%) | High frequency region (eV) | Low frequency region (eV) |
|---|---|---|
| 0.00 | 0.05 | 0.25 |
| 0.05 | 0.09 | 0.37 |
| 0.10 | 0.00 | 0.40 |
| 0.30 | 0.00 | 0.48 |
| 0.50 | 0.06 | 0.26 |

TABLE IV. Activation energies calculated from the Arrhenius plot at low and high frequency region for the temperature range higher than 200 °C.

| Molar system composition (%) | High frequency region (eV) | Low frequency region (eV) |
|---|---|---|
| 0.00 | 0.39 | 0.77 |
| 0.05 | 0.72 | 1.02 |
| 0.10 | 0.71 | 1.06 |
| 0.30 | 0.72 | 1.17 |
| 0.50 | 0.74 | 0.92 |

$$(Cr^{x}_{Sn})_2.O''_{2(ads)}] \xrightarrow{SnO_2} 2(Cr^{x}_{Sn}.O'_{(ads)}), \tag{9}$$

$$Cr^{x}_{Sn}.O'_{(ads)} + Cr'_{Sn} \xrightarrow{SnO_2} (Cr^{x}_{Sn}.)_2O''_{(structural)}. \tag{10}$$

Considering the differences in the activation energies presented in Tables III and IV, the main defects for the SCN system could be $O'_2$ and $O'$, resulting in activation energies of 0.39 and 0.77 eV, respectively. On the other hand, for the SCNCr systems the chromium added promotes the reduction of $O'_2$ to $O'$ and the reduction of $O'$ to $O''$, leading to higher activation energies of 0.72 and 1.02 eV, respectively. The influence of $Cr'_{Sn}$ is to increase the $O'$ and $O''$ adsorption at the grain boundary interface and to promote a decrease in the conductivity by donating electrons to $O_2$ adsorbed at the grain boundary. From these results one may gather that the species that are truly responsible for the barrier formation are $O'$ and $O''$. The $Cr'_{Sn}$ generates the sites to promote the adsorption of electrophylic species. These defects, $O'$ and $O''$, are not equally present at the same grain boundary. One of them is probably predominant at a grain. This behavior leads to a random distribution of both defects, and to different charge transport paths in the sample. If both defects exist at the same grain boundary, only one time constant can be observed, once parallel charge transport paths are created.

All these evidences put together suggest a mechanism for a barrier formation model at the grain boundary of $SnO_2$ based varistor systems analogous to the Gupta and Carlson's barrier model for a multiphase varistor.[17–20] The proposed barrier model is depicted in Fig. 8, where $w$ is the barrier width and $\phi_B$ is the barrier height. Since a new phase precipitation in the grain boundary is not detected, the two barrier tops touch each other.

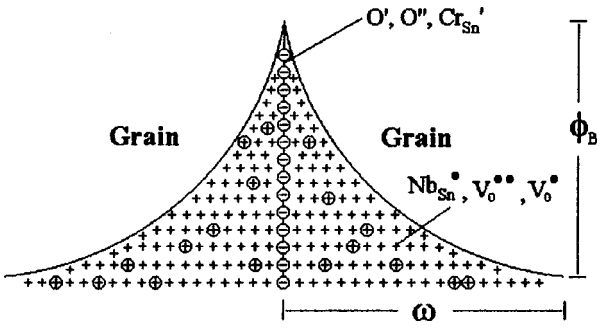


FIG. 8. Schematic representation of the atomic defect model proposed to describe the potential barrier at the grain boundary of $SnO_2$ based varistor systems.

The barrier is formed by the presence of negative defects in the grain boundary region. These defects are mainly $O'$ and $O''$. For temperatures higher than 200 °C, these two defects are the only ones detectable by the impedance measurements. The role of the $Cr_2O_3$ dopant is to improve the adsorption of these electrophylic species at the grain boundary interface.

At this point it is important to describe the change in the energy of activation observed at 200 °C (Tables III and IV). Several explanations are offered in the literature to describe the adsorption mechanism for temperatures lower than 200 °C in the $SnO_2$ sensor system. Chang *et al.*[21] attributed a 0.06 eV energy activation to $Sn_i^{\cdot\cdot}$. Fan *et al.*[22] determined the same activation energy values with $V_O^{\cdot\cdot}$ presence in the system. Egashira *et al.*[23] determined an activation energy of 0.46 eV at 100 °C and attributed it to the water adsorption on the surface. The anomalous behavior at higher temperatures is also described in the literature[11–13] and is discussed as a change in the species adsorbed on the $SnO_2$ surface.

Therefore, the temperature behavior of the impedance data can be described as follow:

(a) For temperatures lower than 200 °C, the presence of $V_O^{\cdot\cdot}$ (Ref. 22) or $Sn_1^{\cdot\cdot}$ (Ref. 21) may be related with the low and high frequency time constants, respectively. Physically adsorbed water[23] should be ruled out once the varistor system is dense.
(b) For higher temperatures, $O'$ and $O''$ are the main adsorbed species at the grain boundary.

It is important to point out that the low activation energy defects detected at temperatures lower than 200 °C are not the main charge carriers in the varistor system. If they were, SCNCr 0.05% would not be a varistor at room temperature since this activation energy is too low. As it is described in the literature,[6] SCNCr 0.05% is a real varistor at room temperatures. Therefore, it is important to explain the differences between the direct current experiments[6] and the data measured with the impedance technique. In the direct current measurements there is a net charge transport. If these low activation defects have a low density, the region becomes saturated rapidly and the charge transport occurs mainly by high activation energy defects. Therefore, the system has varistor behavior at room temperature. On the other hand, these low density defects, i.e., with low activation energy, can be detected using impedance experiments, by the oscillating characteristics of the electric field that leads to no net charge transportation in the oxide.

## CONCLUSIONS

The impedance results show the existence of two time constants in the varistor system investigated. The results suggest different kinds of defects in the grain boundary region. A change in the activation energy at 200 °C was also observed and attributed to the desorption of species previously adsorbed at the grain boundary. Below this temperature one can observe low activation energy defects, which may be related to oxygen vacancies or tin interstitial ions. However, the main charge carriers at all temperature ranges are $O'$ and

$O''$. The presence of $Cr_2O_3$ up to levels of 0.05% improves the varistor properties, generating sites for the adsorption of $O'$ and $O''$ at the grain boundary region. At higher levels, this dopant leads to an increase in the resistivity of the system with no detection of the electric field breakdown.

An atomic defect model for the $SnO_2$ varistor based system can be proposed considering the grain boundary concentration of negative charge defects $(O',O'')$ stabilized by positive charge defects $(Nb_{Sn}^{\cdot}, V_O^{\cdot\cdot}, V_O^{\cdot})$. The role of $Cr_{Sn}^{\prime}$ is to create sites to promote $O'$ and $O''$ defect formation, which are truly responsible for the barrier formation at the grain boundary interface in the grain boundary region.

## ACKNOWLEDGMENTS

The support of this research by CNPq, PADCT/FINEP, and FAPESP is gratefully acknowledged.

[1] Z. M. Jarzebski and J. P. Marton, J. Electrochem. Soc. **123**, 199C (1976).
[2] S. Semanski and T. B. Fryberger, Sens. Actuators B **1**, 97 (1990).
[3] J. Maier and W. Gopel, J. Solid State Chem. **72**, 293 (1988).
[4] W. Gopel, K. D. Shierbaum, and H. D. Wiemhofer, Solid State Ionics **28**, 1631 (1990).
[5] D. E. Willians, in *Solid State Gas Sensors*, edited by A. Hilger (IOP, Bristol, 1987).
[6] S. A. Pianaro, P. R. Bueno, E. Longo, and J. A. Varela, J. Mater. Sci. Lett. **14**, 692 (1995).
[7] E. Almeida, E. C. Pereira, E. Longo, L. O. S. Bulhões, S. A. Pianaro, and J. A. Varela, Química Nova **18**, 301 (1995).
[8] B. A. Boukamp, Solid State Ionics **20**, 31 (1986).
[9] J. M. Wun and C. H. e Lai, J. Am. Ceram. Soc. **74**, 3112 (1991).
[10] Z. M. Jarzebski and J. P. Marton, J. Electrochem. Soc. **123**, 299C (1976).
[11] T. Arai, J. Phys. Soc. Jpn. **15**, 916 (1960).
[12] B. M. Arghirapoulos and S. J. Teichner, J. Catal. **3**, 477 (1964).
[13] Y. Fujita and T. Kwan, J. Res. Inst. Catal. **7**, 24 (1959).
[14] F. Stockmann, Z. Phys. **127**, 563 (1950).
[15] J. A. Cerri, E. R. Leite, D. Gouvea, E. Longo, and J. A. Varela, J. Am. Ceram. Soc. (to be published).
[16] M. C. Kim, K. H. Song, and J. Park, J. Mater. Res. **8**, 1368 (1993).
[17] T. K. Gupta and W. G. Carlson, J. Mater. Sci. **20**, 4091 (1985).
[18] E. R. Leite, J. A. Varela, and E. Longo, J. Appl. Phys. **72**, 147 (1992).
[19] E. R. Leite, J. A. Varela, and E. Longo, J. Mater. Sci. **27**, 5325 (1993).
[20] Y. P. Wang, W. I. Lee, and T. Y. Tseng, Appl. Phys. Lett. **69**, 1807 (1996).
[21] S. C. Chang, J. Vac. Sci. Technol. **17**, 366 (1980).
[22] J. C. Fan and J. B. Goodenough, J. Appl. Phys. **48**, 3524 (1977).
[23] M. Egashira, M. Nakashima, S. Kawasumi, and T. Seiyama, J. Appl. Chem. **85**, 4125 (1981).